On the Seasonal Eddy Variability in the Kuroshio Extension

YANG YANG

School of Marine Sciences, and Center for Ocean-Atmosphere Dynamical Studies, Nanjing University of Information Science and Technology, Nanjing, China

X. SAN LIANG

School of Marine Sciences, and School of Atmospheric Sciences, and Center for Ocean-Atmosphere Dynamical Studies, Nanjing University of Information Science and Technology, Nanjing, China

(Manuscript received 21 March 2018, in final form 28 May 2018)

ABSTRACT

Using a recently developed tool, multiscale window transform (MWT), and the MWT-based canonical energy transfer theory, this study investigates the seasonal eddy variability in the Kuroshio Extension. Distinct seasonal cycles of eddy kinetic energy (EKE) are observed in the upstream and downstream regions of the Kuroshio Extension. In the upstream Kuroshio Extension, the EKE peaks in summer and reaches its minimum in winter over an annual cycle. By diagnosing the spatiotemporal structures of the canonical barotropic and baroclinic energy transfers, we found that internal processes due to mixed instabilities (i.e., both barotropic and baroclinic instabilities) are responsible for the seasonal eddy variability in this region. In the downstream Kuroshio Extension, the EKE exhibits a different annual cycle, peaking in spring and gradually decaying from summer to winter. Significant inverse barotropic energy transfer is found in this region throughout the year, leaving baroclinic instability the primary energy source for the regional seasonal eddy variability. Besides the internal redistribution, it is also evident that the external forcing may influence the Kuroshio Extension EKE seasonality—the EKE is found to be more damped by winds during winter than summer.

1. Introduction

As a continuation of Kuroshio, the inertial jet, namely, the Kuroshio Extension, is dominated by two quasi-stationary meanders, with crests located around 143° and 150°E, respectively (Mizuno and White 1983). Since it is the region where most intense mesoscale eddy activities and air–sea heat exchanges take place in the midlatitude North Pacific, much attention has been paid to understand the dynamics of the Kuroshio Extension and its associated eddies, as well as their potential role in the overlying atmosphere (Qiu and Chen 2005; Pierini 2006; Jayne et al. 2009; Kelly et al. 2010; Waterman et al. 2011; Nakamura et al. 2015; Yang et al. 2017).

It has been identified that there exist significant seasonal variabilities in the regional circulation and ocean heat content in this region (Qiu et al. 1991; Qiu and Kelly 1993; Yasuda et al. 2000; Vivier et al. 2002; Cronin et al. 2013; Lee et al. 2015). In cold seasons (winter and spring), the strength of the Kuroshio Extension's surface transport and its associated southern recirculation reach their minima; meanwhile, the stratification of the upper-layer Kuroshio Extension is rather weak owing to strong local heat loss and wind-stirring mixing, resulting in a steep upper thermocline and a strong sea surface temperature front. During warm seasons (summer and autumn), the intensity of the regional circulation becomes stronger and the steep thermal front structure of the upper ocean is replaced by a flatter and well-stratified upper thermocline.

While previous studies have focused on the seasonality of the current strength and upper-ocean thermal structure in the Kuroshio Extension, less attention has been paid to the seasonal variability of the regional mesoscale eddies. Dynamically, the seasonal modulation of the flow pattern and thermal structure could lead to large changes in the stability properties of the ocean, leaving imprints on the seasonal variation of the regional mesoscale eddy field. Early studies based on short-record altimetry data have reported that the eddy

Corresponding author: X. San Liang, x.san.liang@gmail.com

DOI: 10.1175/JPO-D-18-0058.1

kinetic energy (EKE) level in the Kuroshio Extension peaks in summer and reaches its minimum in winter (Tai and White 1990; Stammer and Wunsch 1999; Ducet and Le Traon 2001; Scharffenberg and Stammer 2010); this has been recently reconfirmed by Zhai (2017) using updated records from 1993 to 2016. So far, the mechanism underlying the seasonal eddy variabilities in the Kuroshio Extension region is still unclear.

Generally, eddy variability in an ocean domain can be influenced by external atmospheric forcing (e.g., wind forcing) or by internal ocean processes such as barotropic and baroclinic instabilities (Stammer and Wunsch 1999; Ferrari and Wunsch 2009). Previous stochastic modeling studies showed evidence of direct eddy generation by fluctuating wind fields (Frankignoul and Müller 1979; Müller and Frankignoul 1981). Since then, several studies have found significant correlations between wind stress variability and EKE in ocean sectors where the background current is relatively weak, for example, the northeastern part of the North Atlantic Ocean (Brachet et al. 2004; White and Heywood 1995; Stammer et al. 2001; Garnier and Schopp 1999). Recently, with the use of satellite-based wind stress and ocean surface geostrophic velocity measurements, several studies claimed that ocean eddies are actually damped by atmospheric winds due to the current feedback on the surface wind stress (e.g., Xu et al. 2016; Renault et al. 2017). Naturally, such damping effect could also vary seasonally and make a contribution to the seasonality of the local EKE.

Internal processes such as barotropic and baroclinic instabilities could potentially control the seasonally varying eddy field in the ocean. Previous idealized models have already shown that changes in the thermal structure by local heat/cooling in the upper ocean can lead to large changes in the baroclinic instability of the mean flow, thus influencing the seasonality of the regional EKE (Legg and McWilliams 2001). A similar scenario has also been found in the observed seasonal EKE modulation in several previous studies (Qiu 1999; Jia et al. 2011; von Appen et al. 2016). On the other hand, as the strength of the regional flow varies seasonally, the barotropic/baroclinic stability properties of the background circulation could also change, providing energy for the generation of mesoscale eddies. The seasonal eddy variation due to flow instabilities is found in many parts of the World Ocean, for example, the Labrador Sea (Eden and Böning 2002), the southeast Indian Ocean (Jia et al. 2011), the North Pacific Subtropical Countercurrent (Chang and Oey 2014; Qiu et al. 2014), the Caribbean Sea (Jouanno et al. 2012), the North Pacific Equatorial Countercurrent (Chen et al. 2015), the Gulf Stream (Kang et al. 2016), and the Red Sea (Zhan et al. 2016).

In this study, we use available satellite observations and ocean reanalysis data to unravel the main factors controlling the seasonality of EKE in the Kuroshio Extension region, with a special focus on the different seasonal EKE phases in the upstream and downstream Kuroshio Extension. The rest of the paper is structured as follows: We first briefly introduce the methods in section 2 and then describe the data in section 3. The major results are presented in section 4. Section 5 summarizes this study.

2. Methods

In this study, a novel localized multiscale energetics analysis with respect to the primitive equations (Liang 2016) is used to explore the seasonal variability of the eddy energy in the Kuroshio Extension. Figure 1 illustrates how different energy reservoirs in a two-scale framework are connected with each other. All the notations in Fig. 1 are explained in Table 1. Readers are referred to Liang (2016) for details. In this study, we focus on the two primary instabilities (i.e., barotropic instability and baroclinic instability) in geophysical fluid dynamics (GFD) by examining the rates of energy transferred from the mean flow to the eddy field; furthermore, the wind work done to the eddy field is also investigated.

Barotropic and baroclinic instabilities are the two primary sources for eddy development in the ocean. These two processes can be quantitatively described by the cross-scale transfers of the kinetic energy and the available potential energy, respectively, from the mean flow into the eddies. As proved in Liang (2016), the cross-scale kinetic energy transfer Γ_K^{ϖ} is given by

$$\Gamma_K^{\varpi} = \frac{1}{2}\left[\widehat{(\mathbf{v}\mathbf{v}_h)}^{\sim\varpi} : \nabla\hat{\mathbf{v}}_h^{\sim\varpi} - \nabla\cdot\widehat{(\mathbf{v}\mathbf{v}_h)}^{\sim\varpi}\cdot\hat{\mathbf{v}}_h^{\sim\varpi}\right]. \tag{1}$$

In (1), the superscript ϖ signifies a specific scale range, or scale window, as called by Liang and Anderson (2007). For this study, we have two windows, that is, the mean flow window and the eddy window. For convenience, they will be signified by $\varpi = 0, 1$ respectively. The vector fields $\mathbf{v}$ and $\mathbf{v}_h$ are the three-dimensional and horizontal velocities. The operator (:) represents the colon product of two dyads (cf. Liang 2016) such that, for four vectors $\mathbf{A}$, $\mathbf{B}$, $\mathbf{C}$, and $\mathbf{D}$,

$$(\mathbf{AB}):(\mathbf{CD}) = (\mathbf{A}\cdot\mathbf{C})(\mathbf{B}\cdot\mathbf{D}).$$

The operator $\widehat{(\cdot)}_n^{\sim\varpi}$ denotes the application of a kind of transform, called multiscale window transform (MWT), of some variable on window ϖ at time step n. The MWT is a new functional analysis tool developed by

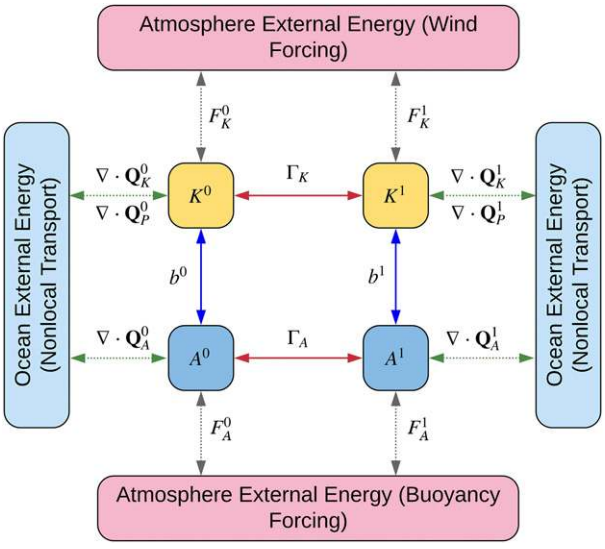

FIG. 1. Schematic of the energy pathway in the MWT-based multiscale energetics formalism (Liang 2016) for a two-window decomposition. Red arrows indicate the energy transfers between the mean-flow window (indicated by superscript 0) and eddy window (indicated by superscript 1), while navy arrows illustrate the buoyancy conversion connecting the KE and APE reservoirs. Green dashed arrows indicate nonlocal processes transporting into or out of the local ocean domain. Gray dashed arrows denote energy exchanges between the ocean and atmosphere. All symbols are illustrated in Table 1.

Liang and Anderson (2007) to fulfill the scale decomposition; it is distinctly different from the existing filters in that it is orthogonal and outputs transform coefficients as well as reconstructed fields (filtered fields), allowing for a faithful representation of multiscale energies, with local information retained. For more about the energy representation problem, see Liang (2016); for technical details about MWT, see Liang and Anderson (2007). By focusing on the high-frequency mesoscale band, we select the eddy window with a period shorter than 1 season (90 days), in accordance with previous findings that the major period of mesoscale eddies in the Kuroshio Extension region is between 4 and 12 weeks (Itoh and Yasuda 2010). Notice that such a cutoff period also effectively removes the seasonal cycle as well as interannual variability of the mean flow.

Likewise, the cross-scale available potential energy transfer Γ_A^{ϖ} proves to be (Liang 2016)

$$\Gamma_A^{\varpi} = \frac{g^2}{2\rho_0^2 N^2}\left[\widehat{(\mathbf{v}\rho)}^{\sim\varpi}\cdot\nabla\hat{\rho}^{\sim\varpi} - \hat{\rho}^{\sim\varpi}\nabla\cdot\widehat{(\mathbf{v}\rho)}^{\sim\varpi}\right], \tag{2}$$

where ρ is the density anomaly, g is the gravitational acceleration, ρ_0 is the constant reference density (1025 kg m^{-3}), and N is the buoyancy frequency. The other symbols

TABLE 1. Symbols for multiscale energetics (ϖ denotes a specific scale window; i.e., $\varpi = 0, 1$). For details, refer to Liang (2016).

K^{ϖ}	Kinetic energy on scale window ϖ
A^{ϖ}	Available potential energy on scale window ϖ
Γ_K	Canonical transfer of kinetic energy
Γ_A	Canonical transfer of available potential energy
b^{ϖ}	Buoyancy conversion on scale window ϖ
$\nabla\cdot\mathbf{Q}_K^{\varpi}$	Advective kinetic energy transport on scale window ϖ
$\nabla\cdot\mathbf{Q}_P^{\varpi}$	Pressure working rate on scale window ϖ
$\nabla\cdot\mathbf{Q}_A^{\varpi}$	Advective available potential energy transport on scale window ϖ
F_K^{ϖ}	Generation of kinetic energy by wind forcing on scale window ϖ
F_A^{ϖ}	Generation of available potential energy by buoyancy forcing on scale window ϖ

are standard. It is important to emphasize that the transfers in (1) and (2) satisfy

$$\sum_{\varpi}\sum_{n}\Gamma_n^{\varpi} = 0, \tag{3}$$

as proved in Liang (2016), where Σ_n and Σ_{ϖ} are the summation over all the sampling time steps n and scale windows ϖ, respectively. [The subscript n is omitted in (1) and (2) for simplicity.] This property, though simple to state, does not hold in classical energetic formalisms. To distinguish it from those one may have encountered in the literature, Γ is called canonical transfer (Liang 2016). Canonical transfer is important in that it is closely related to the classical GFD stabilities: barotropic instability and baroclinic instability (Liang and Anderson 2007). For convenience, we use the superscript $0\to1$ to signify the transfer from the mean flow window ($\varpi = 0$) to the eddy window ($\varpi = 1$). For instance, the canonical kinetic energy (available potential energy) transfer to eddy window ($\varpi = 1$) from the mean flow window ($\varpi = 0$) is denoted as $\Gamma_K^{0\to1}$ ($\Gamma_A^{0\to1}$). As established by Liang and Robinson (2007), a positive $\Gamma_K^{0\to1}$ ($\Gamma_A^{0\to1}$) indicates kinetic energy (available potential energy) transfers from the mean flow to the eddies via barotropic (baroclinic) instability.

The energy transfer between the atmospheric wind and the oceanic eddies is also explored in this study. Within the MWT-based mean flow–eddy decomposition framework, we are able to obtain the rate of eddy wind work (EWW). Following Renault et al. (2017), we calculate the geostrophic EWW since previous studies found that wind work to ageostrophic currents does not feed into the general circulation (Wunsch 1998; von Storch et al. 2007). The EWW is given by

$$\mathrm{EWW} = \frac{1}{\rho_0}\hat{\mathbf{v}}_g^{\sim1}\cdot\hat{\boldsymbol{\tau}}^{\sim1}, \tag{4}$$

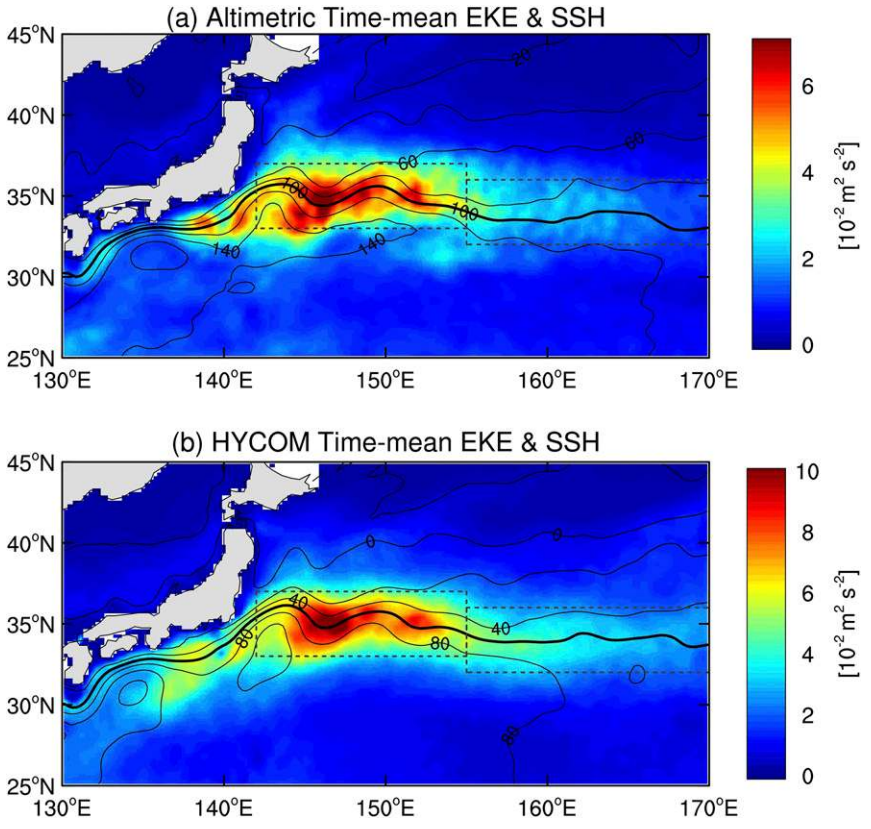

FIG. 2. The long-term mean (1993–2011) maps of EKE (color shading; 10^{-2} m^2 s^{-2}) and SSH (black contours; cm) based on (a) altimetry and (b) the HYCOM reanalysis. The thick line denotes the jet axis. The dashed lines mark the subdomains for the upstream (33°–37°N, 142°–155°E) and downstream (32°–36°N, 155°–170°E) regions.

where $\mathbf{v}_g$ represents the surface geostrophic currents and $\boldsymbol{\tau}$ is the surface wind stress vector.

3. Data

a. HYCOM reanalysis

Outputs from the Hybrid Coordinate Ocean Model with Naval Research Laboratory Coupled Ocean Data Assimilation (HYCOM + NCODA, hereinafter HYCOM for brevity) global 1/12.5° reanalysis are used to estimate the canonical transfer matrices (i.e., $\Gamma_K^{0\to1}$ and $\Gamma_A^{0\to1}$). We choose the HYCOM dataset because it well captures the observed seasonal modulation of the EKE in the Kuroshio Extension region (see section 4a for verification), which is not guaranteed in unconstrained OGCM outputs, owing to the highly nonlinear and stochastic nature of the western boundary current (WBC) system (Yang et al. 2017). HYCOM assimilates a large number of oceanic observations (e.g., the satellite-based sea surface height and sea surface temperature, as well as in situ temperature–salinity profiles) (Cummings 2005). (A more thorough description of the model configuration and how the optimization is carried out can be found at https://hycom.org.) In this study, the 3-day outputs from 1993 to 2011 are used.

b. Satellite observations

Satellite-based datasets over the period of 2000 to 2017 are used to calculate the EWW [i.e., (4)]. The surface geostrophic velocity is obtained from the Copernicus Marine and Environment Monitoring Service (CMEMS), previously distributed by AVISO. The wind stress fields are obtained from the Quick Scatterometer (QuikSCAT) and Advanced Scatterometer (ASCAT) products. In this study, the QuikSCAT data (from 2000 to 2008) and ASCAT data (from 2008 to 2017) are combined to form a long time series. Notice that since the scatterometer directly measures the wind stress, the current effect on the wind stress is thus already included in the wind stress products (Hughes and Wilson 2008; Scott and Xu 2009).

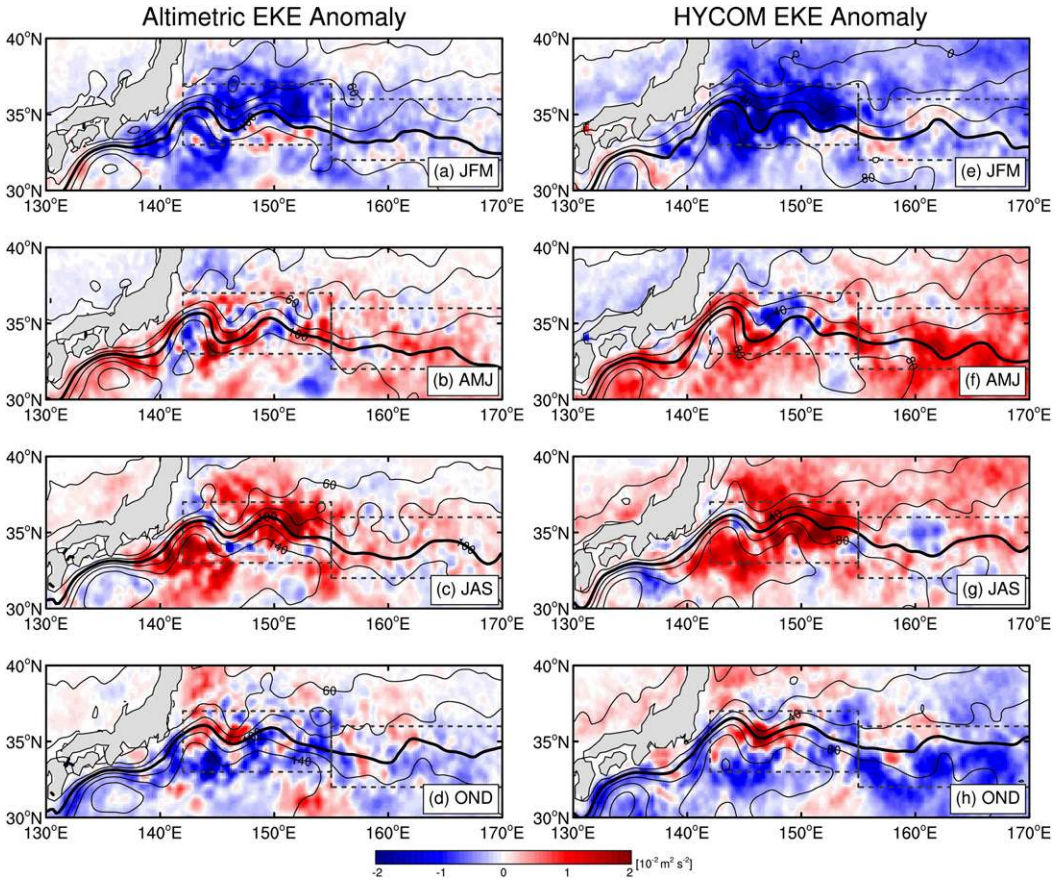

FIG. 3. Seasonal maps of the EKE anomalies (color shading; 10^{-2} m^2 s^{-2}) and SSH (black contours; cm) based on altimetry records in (a) winter (JFM), (b) spring (AMJ), (c) summer (JAS), and (d) autumn (OND). (e)–(h) As in (a)–(d), but for the HYCOM reanalysis.

4. Results

a. Seasonal cycle of EKE

Figure 2 shows the long-term mean maps of the surface geostrophic EKE (color shades) and sea surface height (SSH; black contours) based on the altimetry observation (Fig. 2a) and HYCOM reanalysis (Fig. 2b). Both the horizontal distributions of mean EKE and SSH from HYCOM are in good agreement with the observation. Elevated mesoscale variabilities are found concentrated along the mean path of the eastward jet, with the strongest signal located around the quasi-stationary meanders west of 155°E. The HYCOM also realistically reproduces the seasonal cycle of EKE comparable to the observation. As shown in Fig. 3, the EKE anomalies exhibit a clear annual cycle with maximum in summer months [July–September (JAS)] and minimum in winter months [January–March (JFM)], in agreement with previous studies (Stammer and Wunsch 1999; Scharffenberg and Stammer 2010; Rieck et al. 2015; Zhai 2017).

A closer look at the along-stream EKE variation reveals that the seasonal phases of EKE in upstream and downstream Kuroshio Extension are not quite the same. To demonstrate this, we plot in Fig. 4 the area-mean surface EKE time series averaged over the upstream and downstream Kuroshio Extension boxes as demarcated in Fig. 2 (dashed lines). In the upstream box, the surface EKE has a dominant peak in August, which is revealed in both HYCOM and the altimetry observation (Fig. 4a). In contrast, the area-mean EKE averaged over the downstream box peaks in May and gradually decays from summer to winter (Fig. 4b). It is natural to inquire what causes the difference in seasonality between these two Kuroshio Extension subdomains.

It should be noticed that the amplitude of the EKE simulated by the HYCOM appears consistently larger than that based on the altimetry products. One possible reason for this discrepancy can be attributed to the increased resolution of the numerical model (Sasaki et al. 2017). It is also worth mentioning that finer model resolution might not be the single reason accounting for the

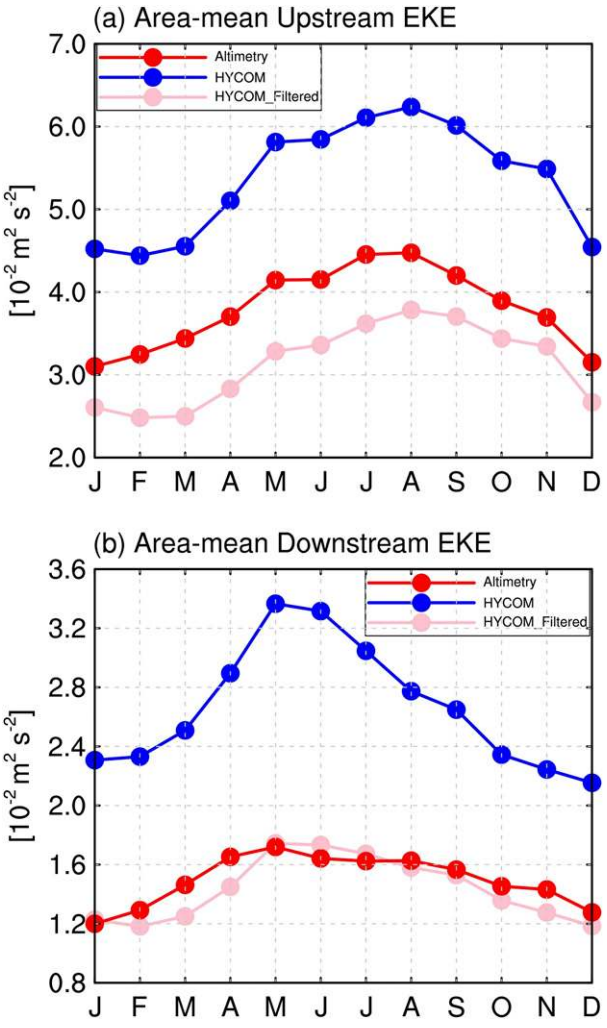

FIG. 4. (a) The seasonal cycle of the area-mean EKE (10^{-2} m^2 s^{-2}) computed from altimetry (red), unadulterated HYCOM output (blue), and spatially filtered HYCOM output (pink) in the upstream Kuroshio Extension. (b) As in (a), but for the downstream Kuroshio Extension region.

overestimated EKE levels in the HYCOM simulation. Previous works have emphasized the important role played by the current feedback on the atmospheric wind stress, which can induce a significant kinetic energy transfer from the oceanic eddies to the atmosphere (e.g., Duhaut and Straub 2006). This damping effect by the wind stress is not captured by ocean-only models such as HYCOM, thus resulting in overestimated EKE levels in the model outputs. Also notice that the downstream EKE seasonality derived from the altimeter observation seems to be less well defined compared to that derived from the HYCOM output (Fig. 4b). This is likely due to the coarse resolution of the altimetry data, which is typically on the order of 150 km in wavelength (Chelton et al. 2011; Qiu et al. 2014). To verify this, we apply a horizontal low-pass filtering to the HYCOM output. The filter is a simple 0.8° running average. An observation is that the magnitude of the resulting EKE is significantly reduced (see the pink lines in Fig. 4). In the downstream region, the seasonality of the HYCOM-derived EKE is substantially reduced after the smoothing, which is now comparable to the altimetry (Fig. 4b). In fact, in a recent study Sasaki et al. (2017) also reported that increased resolution in ocean models not only elevates the kinetic energy level but also increases the amplitude of the EKE seasonality, indicating that finescale ocean processes, such as submesoscale motions, may play important roles in the seasonal variability of the ocean kinetic energy.

To explore the vertical structures of the seasonal eddy variability in the Kuroshio Extension region, Fig. 5 shows the cross-stream sections of the seasonal EKE averaged in the zonal direction of the two subdomains. It can be seen that the seasonal signals of EKE is mainly confined within the upper-600-m water column that has a coherent vertical structure. Again, we note that the mesoscale eddies exhibit a clear difference in seasonality between the upstream and downstream Kuroshio Extension regions. The EKE averaged over the upstream box peaks in summer months (JAS), while in the downstream box it peaks almost one season earlier (i.e., the spring months [April–June (AMJ)]). In the following subsections, we will investigate the underlying dynamics controlling the seasonality of EKE in these two Kuroshio Extension subdomains.

b. Barotropic instability

Barotropic instability is ubiquitous in the WBC systems owing to the presence of strong horizontal shears (Ferrari and Wunsch 2009). In this subsection, we quantify the seasonal evolution of the canonical barotropic transfer (BT) matrix as introduced in section 2. Recall that a positive BT indicates a kinetic energy transfer from the mean flow to the eddies via barotropic instability; conversely, a negative BT indicates an inverse kinetic energy transfer from eddies back to the mean flow.

In Fig. 6, we show the horizontal distributions of the vertically integrated BT (upper 600 m depth) in the four seasons. A general observation is that strong positive and negative BT centers occupy the upstream meander region west of 155°E. Notice that the positive centers tend to appear in areas where the streamlines diverge, and here they happen to be associated with the southward flow due to the upstream confinement of the Japan coast. This is particularly evident in spring and summer. By Rayleigh's theorem (e.g., Pedlosky 1987), for a barotropic jet to lose stability, the gradient of the

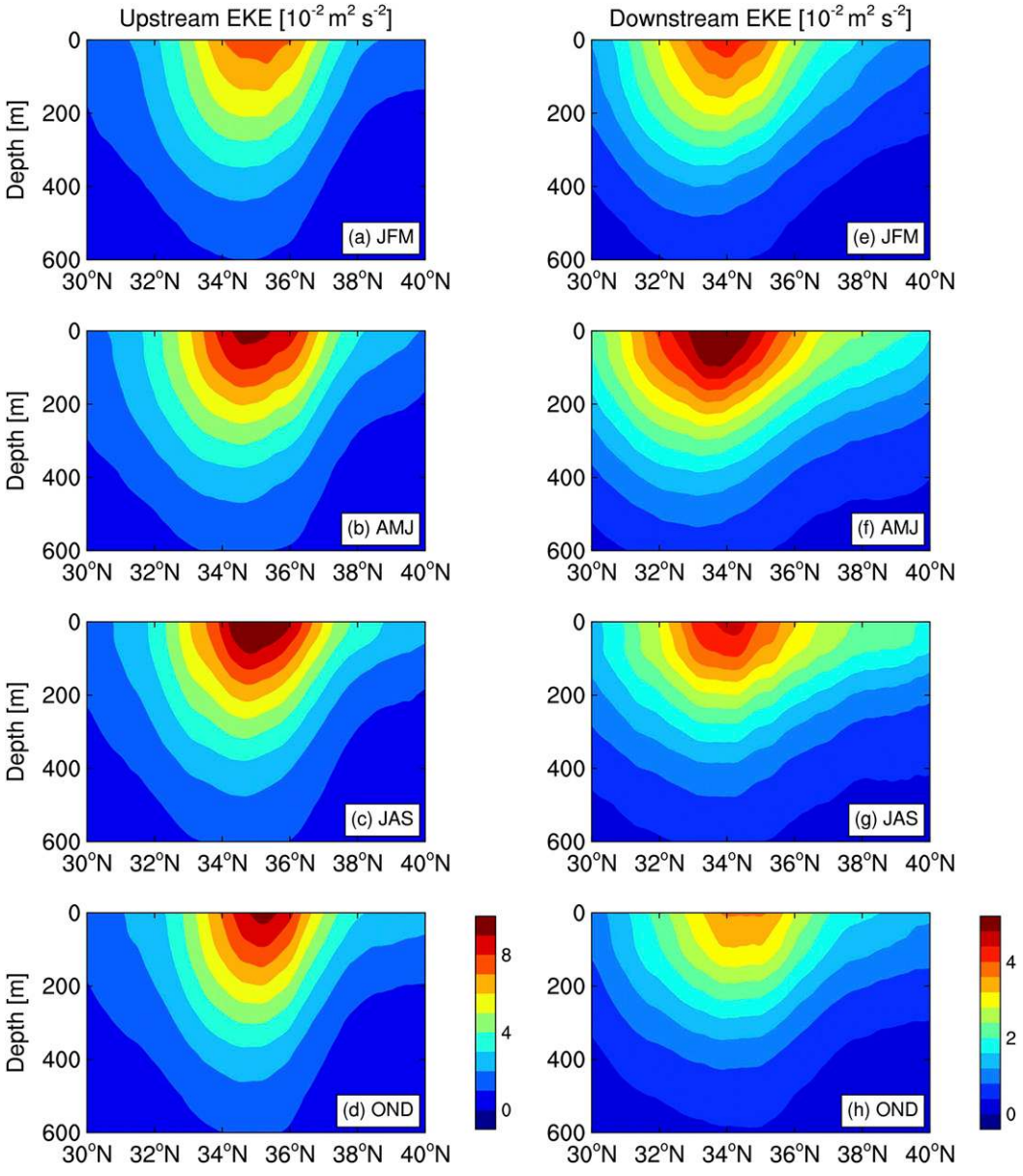

FIG. 5. Vertical structures of the EKE (10^{-2} m^2 s^{-2}) averaged in the zonal direction of the upstream subdomain in (a) winter, (b) spring, (c) summer, and (d) autumn. (e)–(h) As in (a)–(d), but for the downstream subdomain.

background vorticity normal to the jet axis must change sign. When the streamlines diverge, the individual lines will have more chance to meander in their own way, and there may appear more locations for the normal vorticity gradient to change sign. As a result, the jet is more likely to be unstable. To demonstrate this, we plot the normal vorticity gradients at two cross sections of the jet. Section 1 is located at the place where BT is negative, while section 2 is at a place downstream where BT is positive, that is, a place where the flow directs southward; see Fig. 6b. As an example, the corresponding normal vorticity gradients for AMJ are shown in Figs. 7a and 7b. (Those for other months are similar.) Obviously, in Fig. 7b there are much more sign changes across the stream.

We remark that the Rayleigh condition is just a necessary condition for instability; it is not sufficient. In any case, the more sign changes, the larger the possibility for the instability to occur. The drastic change from Fig. 7a to Fig. 7b is a demonstration of this.

Notice that a similar phenomenon has also been discovered with a southward flow in an idealized Antarctic Circumpolar Current model by Youngs et al. (2017),

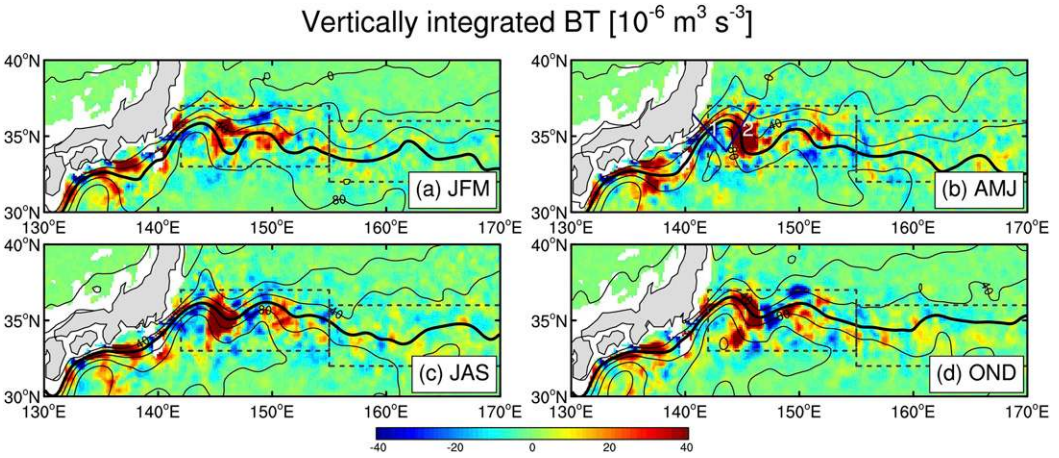

FIG. 6. Seasonal maps of the depth-integrated (upper 600-m depth) barotropic energy transfer (BT) (color shading; $10^{-6}\,m^3\,s^{-3}$) and SSH (black contours; cm) based on HYCOM reanalysis in (a) winter, (b) spring, (c) summer, and (d) autumn. The two blue lines in (b) (labeled 1 and 2) indicate the two cross sections examined in Fig. 7.

who attributed it to the downgradient momentum flux. We remark that it may not be this simple, as the canonical transfer is by far more complicated than some simple momentum flux. In addition, it seems that the atmospheric jet stream over the Pacific Ocean, which has a similar downgradient momentum flux, however has a different instability structure (Zhao and Liang 2018, manuscript submitted to *J. Climate*).

Although surrounded by negative patches, in Fig. 6 the BT is overall positive in the upstream Kuroshio Extension owing to the prevailing positive values confined in the southward-flowing part of the first time-mean meander crest. Regarding its seasonal variations, the positive BT spots become more enhanced during spring and summer, indicating strong EKE production through barotropic instability in these seasons (Figs. 6b,c). In winter, the BT is relatively weak (Fig. 6a), suggesting the mean flow is undergoing a weak barotropic instability during this period of the year.

To illustrate the regional difference of the seasonal cycle of the barotropic energy transfer in the upstream and downstream Kuroshio Extension, we plot in Fig. 8 the cross-stream vertical sectional distributions averaged along the axis in the two subdomains. One can clearly see that strong and positive BT is concentrated along the upstream Kuroshio Extension axis (around 35°N), while weak and negative BT is found in the flanking northern and southern recirculation gyres (Figs. 8a–d). In addition, the seasonal signal of BT matches well with the seasonal evolution of EKE in this subdomain (cf. Figs. 5a–d), indicating that barotropic instability is responsible for the seasonal modulation of EKE in the upstream region of Kuroshio Extension. In contrast, the downstream Kuroshio Extension is characterized by negative BT throughout the year (Figs. 8e–h). A similar scenario in which eddies gain energy from the mean flow in the upstream and lose energy back to the mean current in the downstream Kuroshio Extension has already been reported in previous studies (e.g., Waterman et al. 2011; Yang and Liang 2016).

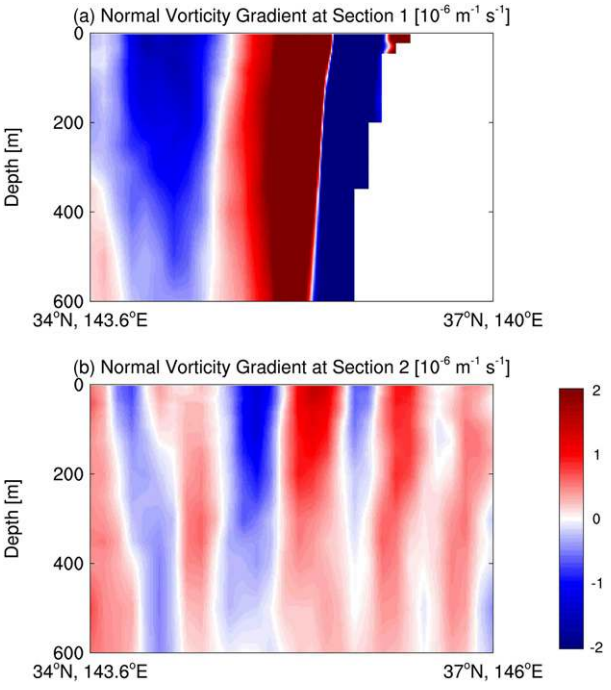

FIG. 7. The vertical structure of the AMJ normal vorticity gradient ($10^{-6}\,m^{-1}\,s^{-1}$) across the two sections as indicated in Fig. 6b.

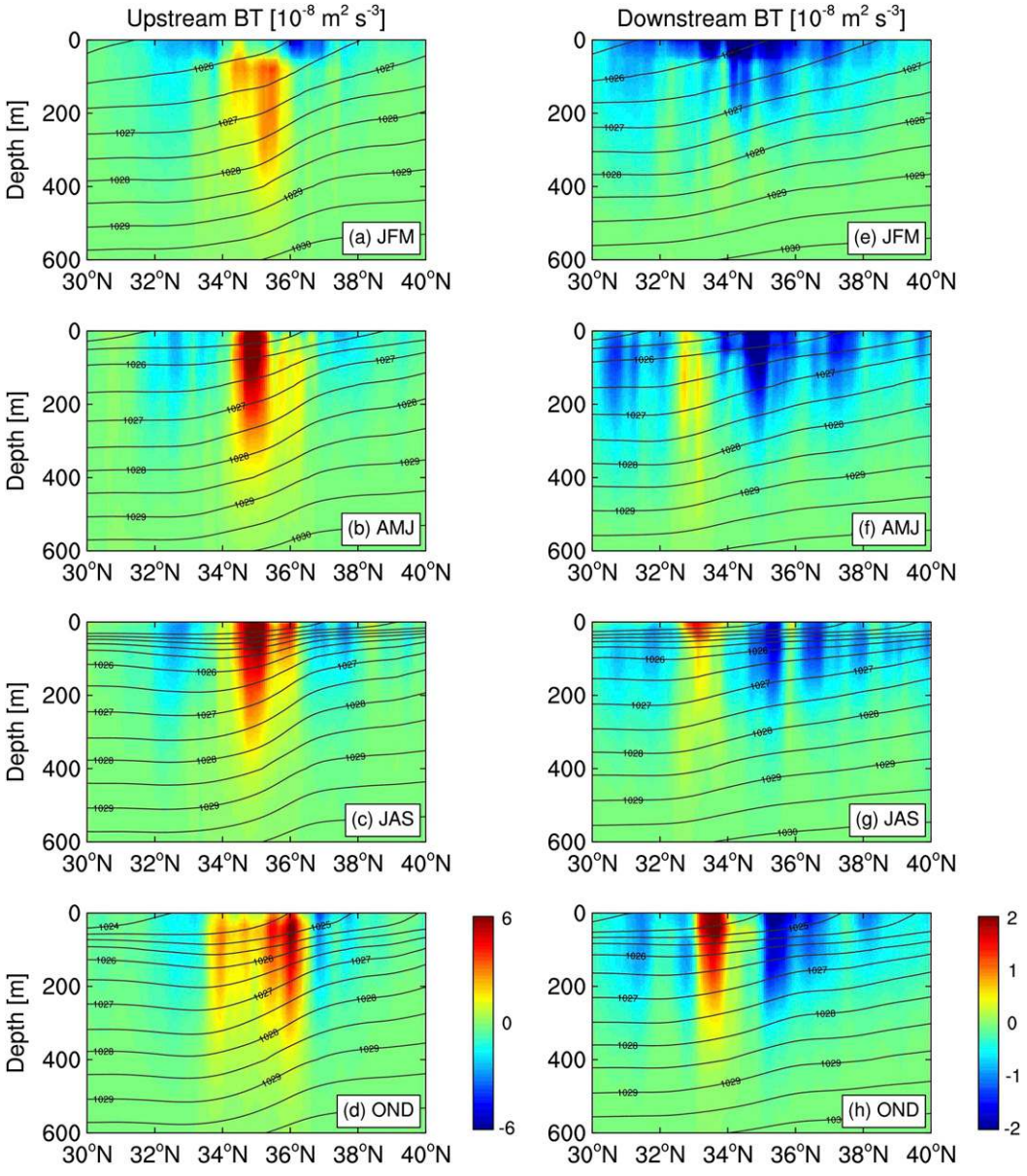

FIG. 8. Vertical structures of BT (color shades; $10^{-8}\,m^2\,s^{-3}$) and density (gray contour; $kg\,m^{-3}$) averaged in the zonal direction of the upstream subdomain in (a) winter, (b) spring, (c) summer, and (d) autumn. (e)–(h) As in (a)–(d), but for the downstream subdomain.

We note that weak and positive BT is confined along the downstream jet axis around 33°–34°N, which reaches its maximum in autumn [October–December (OND)]. This indicates that the seasonal cycle of the EKE in the downstream Kuroshio Extension (which peaks in spring) is not related to the barotropic instability of the mean flow.

c. *Baroclinic instability*

As shown above, barotropic instability plays an important role in forming the EKE seasonality in the upstream Kuroshio Extension region, while in the downstream region, the seasonal variation of barotropic instability is not correlated with that of the EKE. Here we examine the role played by another mechanism, that is, baroclinic instability.

The baroclinic instability of the background flow is quantified by the canonical baroclinic transfer (BC); see section 2 for an introduction. The BC matrix is computed and examined henceforth. Shown in Fig. 9 are the seasonal BC distributions. Unlike BT, the BC maps are dominated by positive values, indicating that baroclinic

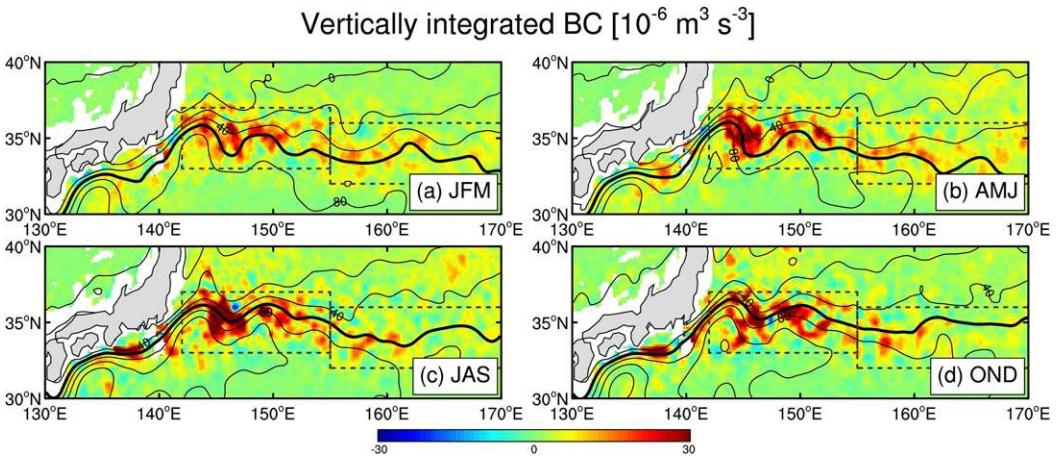

FIG. 9. As in Fig. 6, but for baroclinic energy transfer (BC).

instabilities are widespread in the Kuroshio Extension system. Prevailing baroclinic energy transfer from the mean flow to the eddies are observed in spring and summer months, with the most significant signals occupying the upstream meandering region (Figs. 9b,c). Previous studies also reported similar positive mean-to-eddy available potential energy transfer in this region (Bishop et al. 2013). During the wintertime (JFM), the positive BC is significantly reduced (Fig. 9a).

The left and right columns of Fig. 10 provide the vertical structure of BC in the upstream and downstream subdomains, respectively. Clear seasonal variations are observed; the annual cycles of the upstream and downstream BCs peak in summer and spring, respectively, both of which are in phase with the seasonal modulations of the EKEs in the corresponding subdomains (cf. Fig. 5). This implies that baroclinic instability is responsible for the seasonal variations of the eddy fields in both the upstream and downstream Kuroshio Extension regions. It is noted that enhanced baroclinic energy transfer from the mean flow to the eddies is also found within a shallower water column in the north of the jet during some seasons (e.g., Figs. 10f,g). This baroclinically unstable latitudinal band may be related to the Oyashio Extension accompanied by intense density front therein; we will leave it to future studies. It is also noted that, within the upper 50 m, BC displays a strong winter peak when the upper-layer isopycnals reach their maximum steepness (Figs. 10a,e), while the surface-intensified BC almost disappears during summer when the isopycnals are largely flat (Figs. 10c,g). This indicates that the seasonality of the baroclinic instability within this shallow layer is closely related to the seasonal modulation of the upper-layer density distributions. A detailed investigation of the seasonal cycle of the shallow water baroclinic instability, which is very different from the baroclinic instability in the interior thermocline, and its imprint on the eddy variability is deferred to future studies.

Recent studies have reported that mixed layer instability is responsible for the seasonal cycle of surface-intensified submesoscale processes in the ocean (Boccaletti et al. 2007; Uchida et al. 2017), which further modulates the seasonality of the mesoscale eddies through inverse energy cascades (Qiu et al. 2014; Sasaki et al. 2017). This scenario of submesoscale–mesoscale interaction, however, is not fully resolved in the present 1/12.5° HYCOM reanalysis-data-based analysis. Future studies with higher spatial resolution models and observations are needed to clarify the relative importance to the seasonality of mesoscale EKE between the downscale energy transfer processes due to instabilities and the upscale energy cascades from submesoscale motions.

d. *Wind forcing*

As we reviewed in the introduction, several previous studies have found positive correlations of wind forcing and EKE in low-eddy-energy ocean sectors (Frankignoul and Müller 1979; White and Heywood 1995; Pujol and Larnicol 2005; Yang et al. 2013). However, the scenario of direct eddy generation by local wind forcing is questioned in recent studies of wind work estimates based on finescale scatterometer surface stress observations as well as state-of-the-art coupled ocean–atmosphere models (Duhaut and Straub 2006; Hughes and Wilson 2008; Scott and Xu 2009; Zhai et al. 2012; Xu et al. 2016; Renault et al. 2016). In these studies, the authors found that atmospheric wind acts as an "eddy

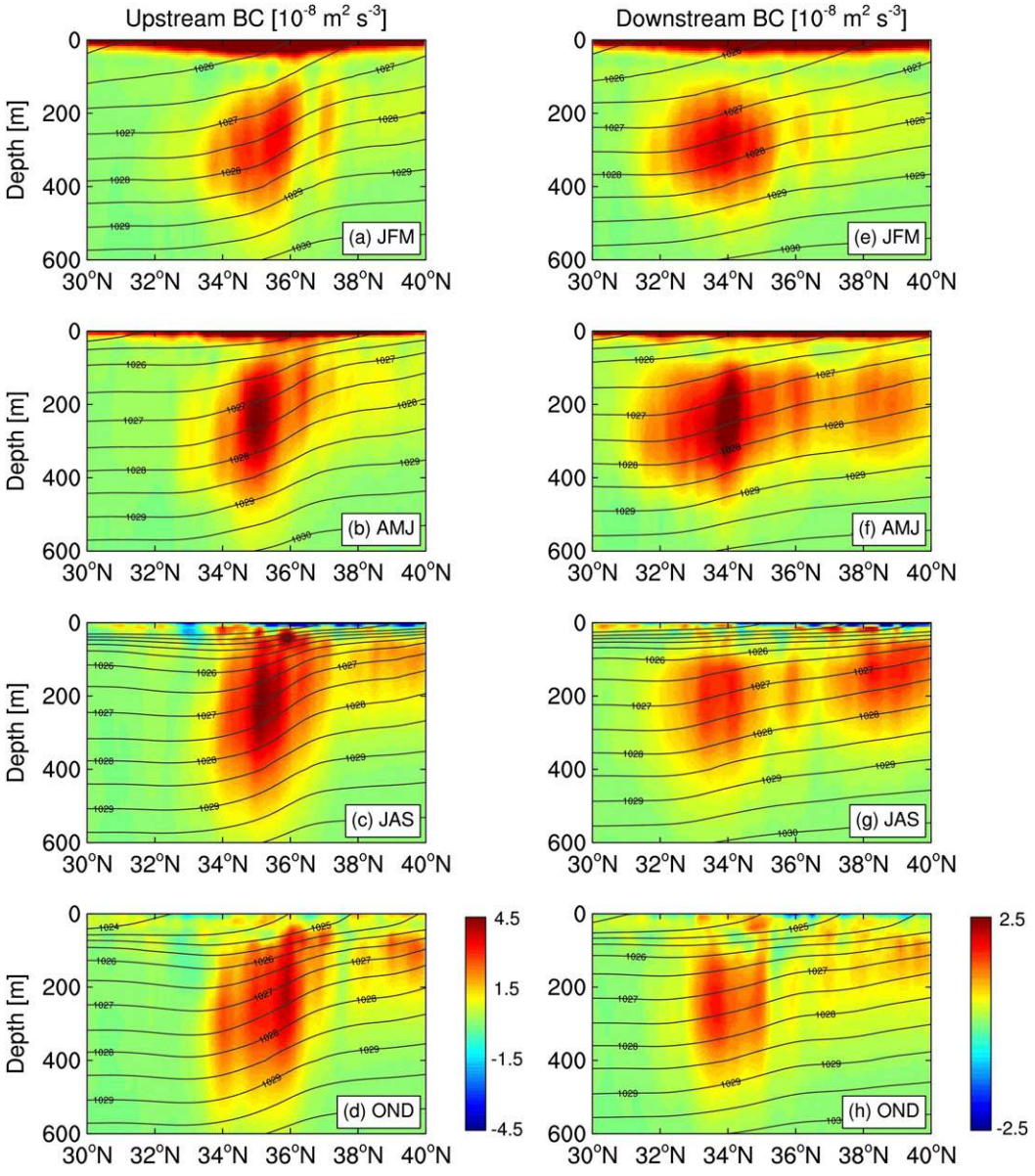

FIG. 10. As in Fig. 8, but for BC.

killer'' rather than an ''eddy generator'' with respect to the current feedback on the surface stress.

Previous studies have recognized that wind work on the ageostrophic flows does not feed into the general circulation (Wunsch 1998; von Storch et al. 2007); we therefore estimate the geostrophic eddy wind work (EWW) using available altimetry and scatterometer data (see more details of data descriptions in section 3). Figure 11 depicts the spatial distributions of the seasonal EWW in the Kuroshio Extension region. The EWW exhibits overwhelming negative values, although mingled with positive patches over the region. This indicates that wind forcing plays an important role to spin down the geostrophic eddies, consistent with previous studies (Hughes and Wilson 2008; Scott and Xu 2009; Zhai et al. 2012; Xu et al. 2016). The negative EWW also presents a well-defined seasonal cycle whose amplitude tends to be larger during the winter season than summer, indicating that more EKE is damped during winter.

e. *Temporal evolution*

To further clarify the relative importance of the above physical processes in determining the seasonal cycle of

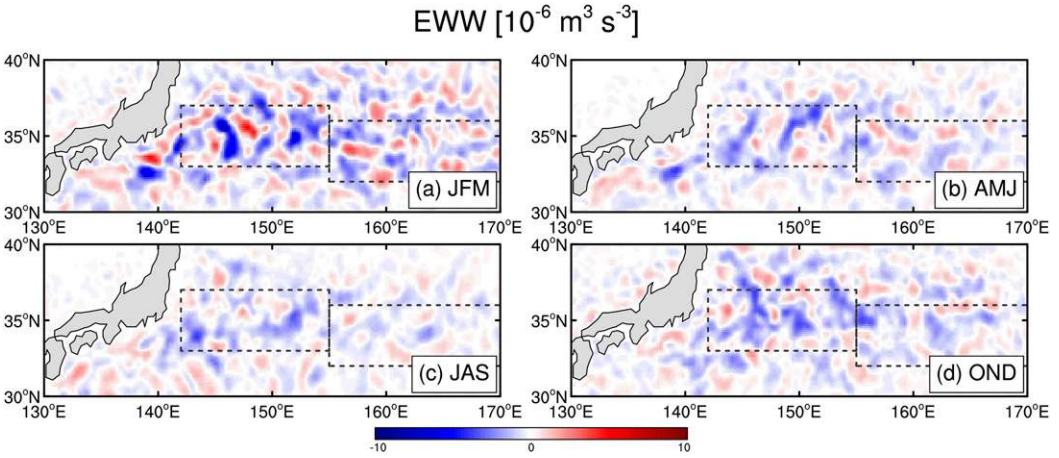

FIG. 11. Seasonal maps of the geostrophic EWW (10^{-6} m^3 s^{-3}) based on altimetry and scatterometer records in (a) winter, (b) spring, (c) summer, and (d) autumn.

the eddy variabilities in the Kuroshio Extension region, we form the area-mean monthly time series of the BC, BT, and EWW averaged over the two Kuroshio Extension subdomains and plot them in Fig. 12. In the upstream Kuroshio Extension, the BC has a sharp peak in July (Fig. 12a). This indicates that the background flow is most baroclinically unstable at this time of the year. The BT, although with a less well-defined annual cycle compared to that of BC, also displays enhanced positive values during late spring through midautumn (Fig. 12a), indicating that barotropic instability is also an important mechanism underlying the seasonal variability of the EKE in this region. In contrast, the downstream subdomain is dominated by pronounced

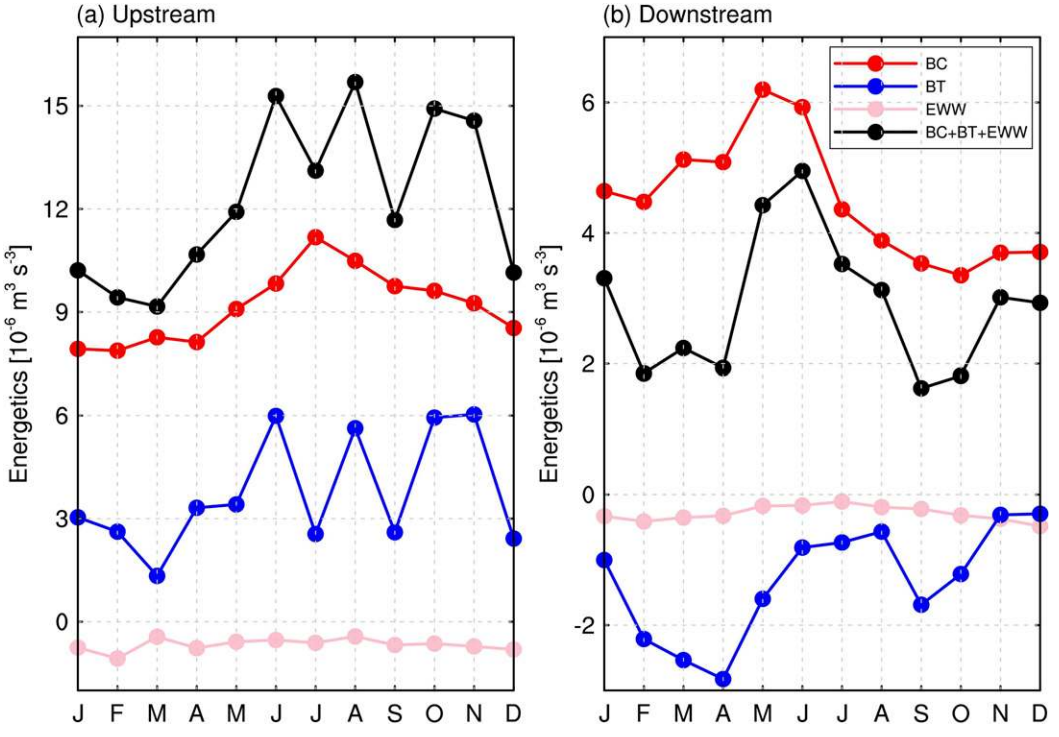

FIG. 12. Annual cycle of the area-mean BC (red), BT (blue), EWW (pink), and the sum of BC, BT, and EWW (black) averaged over the (a) upstream and (b) downstream Kuroshio Extension regions. The units of the energy terms are all in 10^{-6} m^3 s^{-3}.

negative BT throughout the year, implying that the eddies frequently transfer their kinetic energy back to the mean flow (Fig. 12b). Also, the inverse kinetic energy cascade peaks in April and September, which does not correspond to the annual cycle of the downstream EKE; hence, barotropic instability is not responsible for the seasonal cycle of EKE in this region.

The area-mean BC averaged over the downstream box reveals a clear seasonal cycle that resembles that of the EKE (cf. Fig. 12b with Fig. 4b), suggesting that baroclinic instability is the dominant energy source for the seasonal modulation of the eddy field in this region. The EWWs averaged respectively over these two subdomains are negative and reach their maxima in winter and minima in summer, indicating that the damping of EKE by the wind forcing has some effect on the observed EKE seasonality (pink lines in Figs. 12a,b). However, it should be noted that the magnitude of EWW is about one order of magnitude smaller than those of the energy rates caused by the flow instabilities (i.e., BT and BC). That is to say, even if the wind damping is a mechanism for the seasonal EKE variation, its importance is secondary.

5. Conclusions

Using the 1/12.5° HYCOM reanalysis and available satellite observations, this study investigates the possible mechanisms underlying the seasonal modulation of the EKE in the Kuroshio Extension region. Based on a recently developed tool, multiscale window transform (MWT), and the MWT-based canonical energy transfer theory (Liang 2016), our results highlight different mechanisms controlling the seasonal eddy variability in the upstream and downstream Kuroshio Extension regions.

In the upstream Kuroshio Extension, the EKE peaks in summer throughout the upper-600-m water column. The canonical baroclinic energy transfer (BC) has a strong and positive peak in the summer season, whereas the canonical barotropic energy transfer (BT) has enhanced positive values from late spring until mid-autumn. Both BC and BT are significantly weakened during the winter season, resulting in the winter EKE minimum in this subdomain. In other words, mixed instabilities (i.e., both barotropic instability and baroclinic instability) are responsible for the seasonal variability of the eddies in the upstream Kuroshio Extension region.

In the downstream Kuroshio Extension, the regional EKE exhibits a different annual cycle; it peaks in spring and gradually decays from summer to winter. Our results show that the BT here is negative throughout the year and its seasonal phase is not correlated to that of the EKE. In contrast, the BC has a clear seasonal cycle that peaks in spring in this subdomain. This implies that the seasonal evolution of the mesoscale eddies in the downstream Kuroshio Extension is mainly controlled by baroclinic instability.

The seasonal variation of the wind work done to the eddies was also investigated with altimetry and scatterometer observations. It is found that the kinetic energy of the eddies is damped by the wind, consistent with previous studies (Renault et al. 2017). We also found that the damping effect is more enhanced during the winter season; it could be responsible for the winter EKE minimum of the Kuroshio Extension.

It should be noted that, with the present HYCOM reanalysis resolution, submesoscale features are only partially resolved (Uchida et al. 2017). Several recent high-resolution modeling studies, however, have pointed out the positive role played by submesoscale motions in modulating the seasonal variations of mesoscale eddies through strong inverse energy cascades in the North Pacific (Qiu et al. 2014; Sasaki et al. 2014, 2017). This opens the possibility of new mechanisms that control the seasonality of the mesoscale eddies in the Kuroshio Extension region. We look forward to continuing this study with the emerging highly resolved datasets.

Acknowledgments. Yang Yang thanks Peng Zhan, Dong Hu, and Yang Wu for valuable discussions. The HYCOM reanalysis datasets were downloaded from the HYCOM website (https://hycom.org/dataserver/gofs-3pt0/reanalysis). The altimeter products are available at CMEMS (http://www.marine.copernicus.eu), and the scatterometer wind stress data (QuikSCAT+ASCAT) are downloaded from IFREMER (ftp://ftp.ifremer.fr/ifremer/cersat/products/gridded/MWF/L3/). The MS-EVA software is available online (http://www.ncoads.org/). This work was partially supported by the National Science Foundation of China (NSFC) under Grant 41276032, by the 2015 Jiangsu Program of Entrepreneurship and Innovation Group, by Jiangsu Chair Professorship, by the National Program on Global Change and Air-Sea Interaction (GASI-IPOVAI-06), and by NUIST under Grant 2017r054.

REFERENCES

Bishop, S. P., D. R. Watts, and K. A. Donohue, 2013: Divergent eddy heat fluxes in the Kuroshio Extension at 144°–148°E. Part I: Mean structure. *J. Phys. Oceanogr.*, **43**, 1533–1550, https://doi.org/10.1175/JPO-D-12-0221.1.

Boccaletti, G., R. Ferrari, and B. Fox-Kemper, 2007: Mixed layer instabilities and restratification. *J. Phys. Oceanogr.*, **37**, 2228–2250, https://doi.org/10.1175/JPO3101.1.

Brachet, S., P. Y. Le Traon, and C. Le Provost, 2004: Mesoscale variability from a high-resolution model and from altimeter data in the North Atlantic Ocean. *J. Geophys. Res.*, **109**, C12025, https://doi.org/10.1029/2004JC002360.

Chang, Y.-L., and L.-Y. Oey, 2014: Instability of the North Pacific Subtropical Countercurrent. *J. Phys. Oceanogr.*, **44**, 818–833, https://doi.org/10.1175/JPO-D-13-0162.1.

Chelton, D. B., M. G. Schlax, and R. M. Samelson, 2011: Global observations of nonlinear mesoscale eddies. *Prog. Oceanogr.*, **91**, 167–216, https://doi.org/10.1016/j.pocean.2011.01.002.

Chen, X., B. Qiu, S. Chen, Y. Qi, and Y. Du, 2015: Seasonal eddy kinetic energy modulations along the North Equatorial Countercurrent in the western Pacific. *J. Geophys. Res. Oceans*, **120**, 6351–6362, https://doi.org/10.1002/2015JC011054.

Cronin, M. F., and Coauthors, 2013: Formation and erosion of the seasonal thermocline in the Kuroshio Extension Recirculation Gyre. *Deep-Sea Res. II*, **85**, 62–74, https://doi.org/10.1016/j.dsr2.2012.07.018.

Cummings, J. A., 2005: Operational multivariate ocean data assimilation. *Quart. J. Roy. Meteor. Soc.*, **131**, 3583–3604, https://doi.org/10.1256/qj.05.105.

Ducet, N., and P.-Y. Le Traon, 2001: A comparison of surface eddy kinetic energy and Reynolds stresses in the Gulf Stream and the Kuroshio Current Systems from merged TOPEX/Poseidon and ERS-1/2 altimetric data. *J. Geophys. Res.*, **106**, 16 603–16 622, https://doi.org/10.1029/2000JC000205.

Duhaut, T. H. A., and D. N. Straub, 2006: Wind stress dependence on ocean surface velocity: Implications for mechanical energy input to ocean circulation. *J. Phys. Oceanogr.*, **36**, 202–211, https://doi.org/10.1175/JPO2842.1.

Eden, C., and C. Böning, 2002: Sources of eddy kinetic energy in the Labrador Sea. *J. Phys. Oceanogr.*, **32**, 3346–3363, https://doi.org/10.1175/1520-0485(2002)032<3346:SOEKEI>2.0.CO;2.

Ferrari, R., and C. Wunsch, 2009: Ocean circulation kinetic energy: Reservoirs, sources, and sinks. *Annu. Rev. Fluid Mech.*, **41**, 253–282, https://doi.org/10.1146/annurev.fluid.40.111406.102139.

Frankignoul, C., and P. Müller, 1979: Quasi-geostrophic response of an infinite β-plane ocean to stochastic forcing by the atmosphere. *J. Phys. Oceanogr.*, **9**, 104–127, https://doi.org/10.1175/1520-0485(1979)009<0104:QGROAI>2.0.CO;2.

Garnier, V., and R. Schopp, 1999: Wind influence on the mesoscale activity along the Gulf Stream and the North Atlantic currents. *J. Geophys. Res.*, **104**, 18 087–18 110, https://doi.org/10.1029/1999JC900070.

Hughes, C. W., and C. Wilson, 2008: Wind work on the geostrophic ocean circulation: An observational study of the effect of small scales in the wind stress. *J. Geophys. Res.*, **113**, C02016, https://doi.org/10.1029/2007JC004371.

Itoh, S., and I. Yasuda, 2010: Characteristics of mesoscale eddies in the Kuroshio–Oyashio Extension region detected from the distribution of the sea surface height anomaly. *J. Phys. Oceanogr.*, **40**, 1018–1034, https://doi.org/10.1175/2009JPO4265.1.

Jayne, S. R., and Coauthors, 2009: The Kuroshio Extension and its recirculation gyres. *Deep-Sea Res. I*, **56**, 2088–2099, https://doi.org/10.1016/j.dsr.2009.08.006.

Jia, F., L. Wu, and B. Qiu, 2011: Seasonal modulation of eddy kinetic energy and its formation mechanism in the southeast Indian Ocean. *J. Phys. Oceanogr.*, **41**, 657–665, https://doi.org/10.1175/2010JPO4436.1.

Jouanno, J., J. Sheinbaum, B. Barnier, J. M. Molines, and J. Candela, 2012: Seasonal and interannual modulation of the eddy kinetic energy in the Caribbean Sea. *J. Phys. Oceanogr.*, **42**, 2041–2055, https://doi.org/10.1175/JPO-D-12-048.1.

Kang, D., E. N. Curchitser, and A. Rosati, 2016: Seasonal variability of the Gulf Stream kinetic energy. *J. Phys. Oceanogr.*, **46**, 1189–1207, https://doi.org/10.1175/JPO-D-15-0235.1.

Kelly, K. A., R. J. Small, R. M. Samelson, B. Qiu, T. M. Joyce, Y.-O. Kwon, and M. F. Cronin, 2010: Western boundary currents and frontal air–sea interaction: Gulf Stream and Kuroshio Extension. *J. Climate*, **23**, 5644–5667, https://doi.org/10.1175/2010JCLI3346.1.

Lee, E., Y. Noh, B. Qiu, and S.-W. Yeh, 2015: Seasonal variation of the upper ocean responding to surface heating in the North Pacific. *J. Geophys. Res. Oceans*, **120**, 5631–5647, https://doi.org/10.1002/2015JC010800.

Legg, S., and J. C. McWilliams, 2001: Convective modifications of a geostrophic eddy field. *J. Phys. Oceanogr.*, **31**, 874–891, https://doi.org/10.1175/1520-0485(2001)031<0874:CMOAGE>2.0.CO;2.

Liang, X. S., 2016: Canonical transfer and multiscale energetics for primitive and quasigeostrophic atmospheres. *J. Atmos. Sci.*, **73**, 4439–4468, https://doi.org/10.1175/JAS-D-16-0131.1.

——, and D. G. M. Anderson, 2007: Multiscale window transform. *Multiscale Model. Simul.*, **6**, 437–467, https://doi.org/10.1137/06066895X.

——, and A. R. Robinson, 2007: Localized multi-scale energy and vorticity analysis: II. Finite-amplitude instability theory and validation. *Dyn. Atmos. Oceans*, **44**, 51–76, https://doi.org/10.1016/j.dynatmoce.2007.04.001.

Mizuno, K., and W. B. White, 1983: Annual and interannual variability in the Kuroshio Current System. *J. Phys. Oceanogr.*, **13**, 1847–1867, https://doi.org/10.1175/1520-0485(1983)013<1847:AAIVIT>2.0.CO;2.

Müller, P., and C. Frankignoul, 1981: Direct atmospheric forcing of geostrophic eddies. *J. Phys. Oceanogr.*, **11**, 287–308, https://doi.org/10.1175/1520-0485(1981)011<0287:DAFOGE>2.0.CO;2.

Nakamura, H., A. Isobe, S. Minobe, H. Mitsudera, M. Nonaka, and T. Suga, 2015: ''Hot spots'' in the climate system—New developments in the extratropical ocean–atmosphere interaction research: A short review and an introduction. *J. Oceanogr.*, **71**, 463–467, https://doi.org/10.1007/s10872-015-0321-5.

Pedlosky, J., 1987: *Geophysical Fluid Dynamics*. 2nd ed. Springer-Verlag, 710 pp.

Pierini, S., 2006: A Kuroshio Extension system model study: Decadal chaotic self-sustained oscillations. *J. Phys. Oceanogr.*, **36**, 1605–1625, https://doi.org/10.1175/JPO2931.1.

Pujol, M.-I., and G. Larnicol, 2005: Mediterranean Sea eddy kinetic energy variability from 11 years of altimetric data. *J. Mar. Syst.*, **58**, 121–142, https://doi.org/10.1016/j.jmarsys.2005.07.005.

Qiu, B., 1999: Seasonal eddy field modulation of the North Pacific Subtropical Countercurrent: TOPEX/Poseidon observations and theory. *J. Phys. Oceanogr.*, **29**, 2471–2486, https://doi.org/10.1175/1520-0485(1999)029<2471:SEFMOT>2.0.CO;2.

——, and K. A. Kelly, 1993: Upper-ocean heat balance in the Kuroshio Extension region. *J. Phys. Oceanogr.*, **23**, 2027–2041, https://doi.org/10.1175/1520-0485(1993)023<2027:UOHBIT>2.0.CO;2.

——, and S. Chen, 2005: Variability of the Kuroshio Extension jet, recirculation gyre, and mesoscale eddies on decadal time scales. *J. Phys. Oceanogr.*, **35**, 2090–2103, https://doi.org/10.1175/JPO2807.1.

——, K. A. Kelly, and T. M. Joyce, 1991: Mean flow and variability in the Kuroshio Extension from Geosat altimetry data. *J. Geophys. Res.*, **96**, 18 491–18 507, https://doi.org/10.1029/91JC01834.

——, S. Chen, P. Klein, H. Sasaki, and Y. Sasai, 2014: Seasonal mesoscale and submesoscale eddy variability along the North

Pacific Subtropical Countercurrent. *J. Phys. Oceanogr.*, **44**, 3079–3098, https://doi.org/10.1175/JPO-D-14-0071.1.

Renault, L., M. J. Molemaker, J. C. McWilliams, A. F. Shchepetkin, F. Lemarié, D. Chelton, S. Illig, and A. Hall, 2016: Modulation of wind work by oceanic current interaction with the atmosphere. *J. Phys. Oceanogr.*, **46**, 1685–1704, https://doi.org/10.1175/JPO-D-15-0232.1.

——, J. C. McWilliams, and S. Masson, 2017: Satellite observations of imprint of oceanic current on wind stress by air-sea coupling. *Sci. Rep.*, **7**, 17747, https://doi.org/10.1038/s41598-017-17939-1.

Rieck, J. K., C. W. Böning, R. J. Greatbatch, and M. Scheinert, 2015: Seasonal variability of eddy kinetic energy in a global high-resolution ocean model. *Geophys. Res. Lett.*, **42**, 2015GL066152, https://doi.org/10.1002/2015GL066152.

Sasaki, H., P. Klein, B. Qiu, and Y. Sasai, 2014: Impact of oceanic-scale interactions on the seasonal modulation of ocean dynamics by the atmosphere. *Nat. Commun.*, **5**, 5636, https://doi.org/10.1038/ncomms6636.

——, ——, Y. Sasai, and B. Qiu, 2017: Regionality and seasonality of submesoscale and mesoscale turbulence in the North Pacific Ocean. *Ocean Dyn.*, **67**, 1195–1216, https://doi.org/10.1007/s10236-017-1083-y.

Scharffenberg, M. G., and D. Stammer, 2010: Seasonal variations of the large-scale geostrophic flow field and eddy kinetic energy inferred from the TOPEX/Poseidon and Jason-1 tandem mission data. *J. Geophys. Res.*, **115**, C02008, https://doi.org/10.1029/2008JC005242.

Scott, R. B., and Y. Xu, 2009: An update on the wind power input to the surface geostrophic flow of the World Ocean. *Deep-Sea Res. I*, **56**, 295–304, https://doi.org/10.1016/j.dsr.2008.09.010.

Stammer, D., and C. Wunsch, 1999: Temporal changes in eddy energy of the oceans. *Deep-Sea Res. II*, **46**, 77–108, https://doi.org/10.1016/S0967-0645(98)00106-4.

——, C. Böning, and C. Dieterich, 2001: The role of variable wind forcing in generating eddy energy in the North Atlantic. *Prog. Oceanogr.*, **48**, 289–311, https://doi.org/10.1016/S0079-6611(01)00008-8.

Tai, C.-K., and W. B. White, 1990: Eddy variability in the Kuroshio Extension as revealed by Geosat altimetry: Energy propagation away from the jet, Reynolds stress, and seasonal cycle. *J. Phys. Oceanogr.*, **20**, 1761–1777, https://doi.org/10.1175/1520-0485(1990)020<1761:EVITKE>2.0.CO;2.

Uchida, T., R. Abernathey, and S. Smith, 2017: Seasonality of eddy kinetic energy in an eddy permitting global climate model. *Ocean Modell.*, **118**, 41–58, https://doi.org/10.1016/j.ocemod.2017.08.006.

Vivier, F., K. A. Kelly, and L. A. Thompson, 2002: Heat budget in the Kuroshio Extension region: 1993–99. *J. Phys. Oceanogr.*, **32**, 3436–3454, https://doi.org/10.1175/1520-0485(2002)032<3436:HBITKE>2.0.CO;2.

von Appen, W.-J., U. Schauer, T. Hattermann, and A. Beszczynska-Möller, 2016: Seasonal cycle of mesoscale instability of the West Spitsbergen Current. *J. Phys. Oceanogr.*, **46**, 1231–1254, https://doi.org/10.1175/JPO-D-15-0184.1.

von Storch, J.-S., H. Sasaki, and J. Marotzke, 2007: Wind-generated power input to the deep ocean: An estimate using a 1/10° general circulation model. *J. Phys. Oceanogr.*, **37**, 657–672, https://doi.org/10.1175/JPO3001.1.

Waterman, S., N. G. Hogg, and S. R. Jayne, 2011: Eddy–mean flow interaction in the Kuroshio Extension region. *J. Phys. Oceanogr.*, **41**, 1182–1208, https://doi.org/10.1175/2010JPO4564.1.

White, M. A., and K. J. Heywood, 1995: Seasonal and interannual changes in the North Atlantic subpolar gyre from Geosat and TOPEX/Poseidon altimetry. *J. Geophys. Res.*, **100**, 24 931–24 941, https://doi.org/10.1029/95JC02123.

Wunsch, C., 1998: The work done by the wind on the oceanic general circulation. *J. Phys. Oceanogr.*, **28**, 2332–2340, https://doi.org/10.1175/1520-0485(1998)028<2332:TWDBTW>2.0.CO;2.

Xu, C., X. Zhai, and X.-D. Shang, 2016: Work done by atmospheric winds on mesoscale ocean eddies. *Geophys. Res. Lett.*, **43**, 12 174–12 180, https://doi.org/10.1002/2016GL071275.

Yang, H., L. Wu, H. Liu, and Y. Yu, 2013: Eddy energy sources and sinks in the South China Sea. *J. Geophys. Res. Oceans*, **118**, 4716–4726, https://doi.org/10.1002/jgrc.20343.

Yang, Y., and X. S. Liang, 2016: The instabilities and multiscale energetics underlying the mean–interannual–eddy interactions in the Kuroshio Extension region. *J. Phys. Oceanogr.*, **46**, 1477–1494, https://doi.org/10.1175/JPO-D-15-0226.1.

——, ——, B. Qiu, and S. Chen, 2017: On the decadal variability of the eddy kinetic energy in the Kuroshio Extension. *J. Phys. Oceanogr.*, **47**, 1169–1187, https://doi.org/10.1175/JPO-D-16-0201.1.

Yasuda, I., T. Tozuka, M. Noto, and S. Kouketsu, 2000: Heat balance and regime shifts of the mixed layer in the Kuroshio Extension. *Prog. Oceanogr.*, **47**, 257–278, https://doi.org/10.1016/S0079-6611(00)00038-0.

Youngs, M. K., A. F. Thompson, A. Lazar, and K. J. Richards, 2017: ACC meanders, energy transfer, and mixed barotropic–baroclinic instability. *J. Phys. Oceanogr.*, **47**, 1291–1305, https://doi.org/10.1175/JPO-D-16-0160.1.

Zhai, X., 2017: The annual cycle of surface eddy kinetic energy and its influence on eddy momentum fluxes as inferred from altimeter data. *Satell. Oceanogr. Meteor.*, **2**, 299, https://doi.org/10.18063/som.v2i2.299.

——, H. L. Johnson, D. P. Marshall, and C. Wunsch, 2012: On the wind power input to the ocean general circulation. *J. Phys. Oceanogr.*, **42**, 1357–1365, https://doi.org/10.1175/JPO-D-12-09.1.

Zhan, P., A. C. Subramanian, F. Yao, A. R. Kartadikaria, D. Guo, and I. Hoteit, 2016: The eddy kinetic energy budget in the Red Sea. *J. Geophys. Res. Oceans*, **121**, 4732–4747, https://doi.org/10.1002/2015JC011589.